



Review

Recent Advances in Graphene-Based Mesoporous Nanosheets for Supercapacitors

Wenbei Bo ^{1,†}, Hongtao Zhang ^{1,†}, Guocheng Yin ^{2,†}, Liangzhu Zhang ^{3,*} and Jieqiong Qin ^{1,*} 

¹ College of Science, Henan Agricultural University, 63 Agricultural Road, Zhengzhou 450002, China; bowenbei08@163.com (W.B.); 13525861781@163.com (H.Z.)

² School of Chemistry and Environmental Engineering, Institute of Advanced Functional Materials for Energy, Jiangsu University of Technology, Changzhou 213001, China; ygc_012023@163.com

³ School of Materials Science and Engineering, East China University of Science and Technology, Shanghai 200237, China

* Correspondence: zhangliangzhu@ecust.edu.cn (L.Z.); qinjieqiong@henau.edu.cn (J.Q.)

† These authors contributed equally to this work.

Abstract: Among typical energy storage devices, supercapacitors play a predominant role in industry and our life owing to their rapid charge/discharge rate, superior lifespan, high power density, low cost, and outstanding safety. However, their low energy density has severely hindered their further development. For active electrode materials, graphene-based mesoporous nanosheets (GMNs) can combine the advantages from graphene and mesoporous materials, which can be applied to significantly enhance the energy density of supercapacitors. Here, we review the recent advances in GMNs for supercapacitors, focusing on in-plane mesoporous graphene and sandwich-like graphene-based heterostructures. Firstly, the synthesis of in-plane mesoporous graphene with ordered and disordered mesopores for supercapacitors is introduced. Secondly, sandwich-like graphene-based heterostructures are classified into mesoporous carbon/graphene, mesoporous heteroatom-doped carbon/graphene, mesoporous conducting polymer/graphene, and mesoporous metal oxide/graphene, and their applications in supercapacitors are discussed in detail. Finally, the challenges and opportunities of GMNs for high-performance supercapacitors are proposed.

Keywords: two-dimensional; mesoporous materials; graphene; supercapacitors; energy storage



Citation: Bo, W.; Zhang, H.; Yin, G.; Zhang, L.; Qin, J. Recent Advances in Graphene-Based Mesoporous Nanosheets for Supercapacitors. *C* **2023**, *9*, 91. <https://doi.org/10.3390/c9040091>

Academic Editors: Jesús Iniesta and Alicia Gomis-Berenguer

Received: 23 August 2023

Revised: 22 September 2023

Accepted: 25 September 2023

Published: 27 September 2023



Copyright: © 2023 by the authors. Licensee MDPI, Basel, Switzerland. This article is an open access article distributed under the terms and conditions of the Creative Commons Attribution (CC BY) license (<https://creativecommons.org/licenses/by/4.0/>).

1. Introduction

In recent years, the rapid consumption of fossil fuels has resulted in energy shortages and environmental issues. Therefore, the development of alternative energy sources (such as wind, solar, and tidal energy) and their effective storage technologies is vital [1–6]. At present, electrochemical energy storage systems including batteries and supercapacitors (SCs) are considered some of the important ways to store renewable energy [7–9]. Especially, SCs have sparked a wide range of interest because of their fast charge/discharge rate, long life, high power density, and high safety [10–18]. Based on the energy storage mechanism, SCs are classified into electric double-layer capacitors and pseudocapacitors. The former are mainly based on the physical adsorption/desorption that occurs on the surface of electrodes, while the latter store charge through surface and near-surface redox reactions [19,20].

To enhance the energy density of SCs, various electrode materials have been exploited [9,21–23], in which graphene stands out. Graphene is a 2D carbonaceous substance composed of sp² hybrid carbon atoms arranged in a honeycomb crystal structure [24]. Since it was discovered by Geim and Novoselov in 2004, graphene is considered as the hardest and thinnest 2D material with a sheet thickness of 0.34 nm [25]. Notably, graphene possesses an atomic-level thinness, large theoretical surface area (2630 m²/g), numerous active sites, excellent electrical conductivity, rapid ion–electron transport, and impressive

specific capacitance, thus making it promising in the field of energy storage and conversion, especially SCs. As an active electrode material and conductive substance, graphene ensures good electrical conductivity, accessible contact area, superior ion transport capability, and excellent flexibility, resulting in enhanced electrochemical performance for the corresponding SCs.

However, the van der Waals forces between different layers results in the easy self-stacking of graphene nanosheets and obvious decrease in specific surface area (SSA) and active sites, which hinder ion transport and lead to a significant reduction in electrochemical performance [26–32]. Considering that mesoporous materials possess a high SSA, large pore volume, and tunable nanostructure [22,33–36], introducing the mesopore structure into graphene to customize graphene-based mesoporous nanosheets (GMNs) will integrate the merits of graphene and mesoporous materials, restrain the restacking of graphene layers, and realize new physiochemical properties [37–40]. Therefore, GMNs are regarded as one ideal electrode material for high-performance SCs. Specifically, the mesopores can serve as ion transfer channels to reduce the diffusion resistance of electrolyte ions and thus realize good rate performance and power density for the SCs. Additionally, the mesopore networks endow GMNs with improved specific surface areas and active sites, as well as large pore volumes and reaction spaces. The high SSAs and abundant active sites enable electrolyte ions to be fully embedded and increase the effective contact area between the electrode and electrolyte, which can enhance the specific capacitance and energy density of the corresponding SCs. The large pore volume and sufficient reaction space can accommodate solvated electrolyte ions and buffer the volume change of the electrode during the charging/discharging process, delivering good cycling stability for the SCs [23,38,39,41–47]. Ultimately, these structural advantages endow GMNs with a high specific capacitance, good rate capacity, exceptional cycling stability, and improved power and energy densities for SCs. Although recent advances in graphene for energy storage and conversion have been summarized [48–50], a comprehensive overview of the synthesis and SC applications of GMNs is still lacking.

Herein, this review systematically presents recent advances in GMNs for SCs (Figure 1). In particular, GMNs include in-plane mesoporous graphene and sandwich-like graphene-based heterostructures. Based on the different degree of mesopore ordering, GMNs can also be divided into ordered GMNs and disordered GMNs. Therefore, the synthesis and SC applications of in-plane mesoporous graphene with ordered and random mesopores are firstly introduced. Further, various sandwich-like graphene-based heterostructures, e.g., mesoporous carbon/graphene, mesoporous heteroatom-doped carbon/graphene, mesoporous conducting polymer/graphene, and mesoporous metal oxide/graphene, are summarized for SCs. Finally, the challenges and opportunities of GMNs and the corresponding SCs in the future are provided.

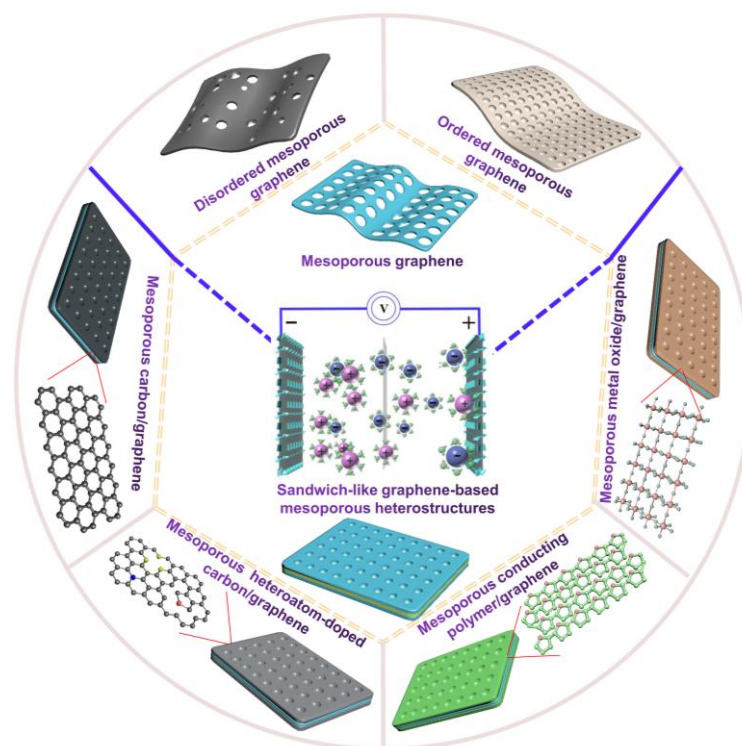


Figure 1. Schematic diagram of various GMNs for SCs.

2. Mesoporous Graphene

Compared with conventional graphene nanosheets, mesoporous graphene with planar vertical holes not only guarantees a higher SSA, but also possesses unimpeded transport channels in the vertical and horizontal directions, leading to a greatly increasing mass transfer rate [51–53]. Hence, its preparation and application in SCs are attracting more attention [53–58]. According to the degree of mesopore ordering, we classify mesoporous graphene into two categories in this section, disordered and ordered.

2.1. Disordered Mesoporous Graphene

For disordered mesoporous graphene, the pore size has a wide distribution range and the pore shape is relatively irregular [59–61]. Physical (photo/electron/plasma) etching has been employed for the creation of mesoporous mono/multi-layer graphene. For example, Guerra et al. reported controllable defect creation in isotopically labeled bilayer graphene through oxygen plasma treatment [62]. The high-resolution transmission electron microscopy (HRTEM) confirmed randomly distributed holes of a few nanometers, namely the vacancy defects caused by the oxygen plasma. This work provided a simple and effective method for controlling the density of defects in multi-layer graphene through sample positioning combined with the oxygen plasma. Chemical etching is also considered as one of most common and reliable methods to prepare mesoporous graphene [63,64]. In addition, various approaches have been proposed, including ion irradiation [65], hydrothermal reaction [66,67], the template function [33,68], chemical vapor deposition [69], and so on [70]. But these methods frequently result in very low yields and involve a difficult handling process, highlighting the necessity for the development of new, scalable synthesis strategies. As an example, Kim et al. [71] explored the universal synthesis of graphene nanomeshes (GNMs) through catalytic carbon gasification (Figure 2a). Specifically, graphene oxide (GO) nanosheets were selectively etched by metal oxide (i.e., SnO_2 , Fe_3O_4 , and RuO_2) nanoparticles, and then HI was selected to remove metal oxides and reduce GO. Notably, by varying the size and proportion of metal oxide on the graphene, the pore size, pore density distribution, and neck size of GNMs could be readily controlled. Using 7 wt%, 11 wt%, and 17 wt% SnO_2 , the porosity distribution of GNMs was regulated between 500

and $5000 \mu\text{m}^{-2}$. When the catalytic SnO_2 was replaced by Fe_3O_4 and RuO_2 , the pore size of GNMs could be regulated from 5 to 20 nm. Finally, the GNMs as electrode materials of SCs exhibited superior electrochemical properties, mainly including an exceptional capacitance of 253 F/g at 1 A/g, high rate capability of 212 F/g at 100 A/g, and impressive cycle stability of 91% of retention after 50,000 cycles.

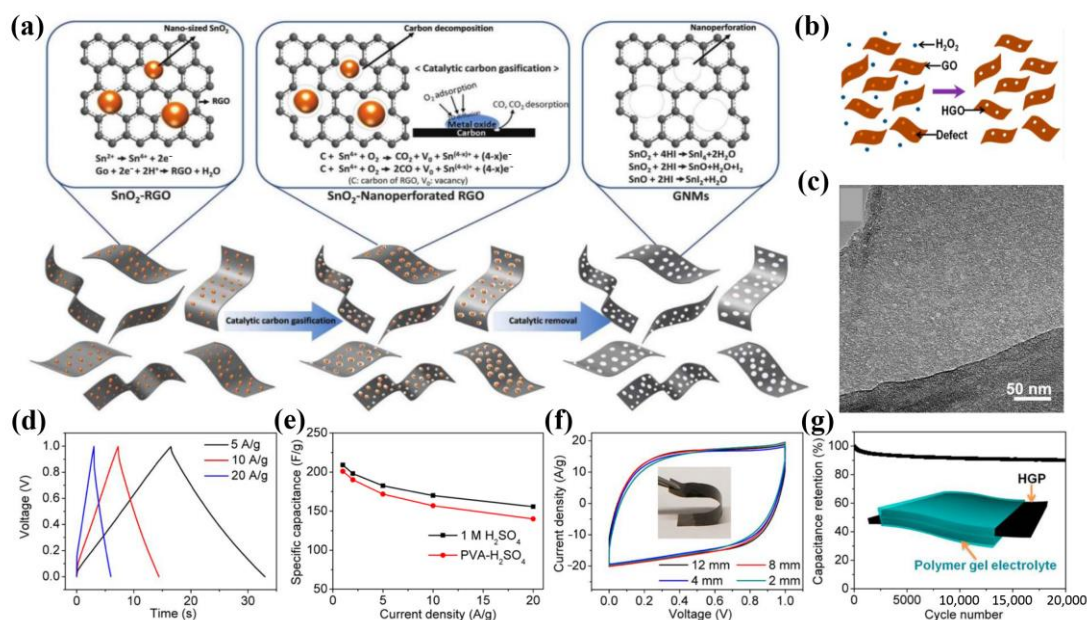


Figure 2. (a) Schematic illustration of the preparation of GNMs [71]. (b) Fabrication mechanism and (c) TEM image of HGO, (d) galvanostatic charge/discharge (GCD) profiles, (e) specific capacitance versus current density, (f) cyclic voltammetry (CV) curves at different bending radii, and (g) cycling stability at 10 A/g and bending radius of ~ 2 mm of HGO-based SCs [72].

Analogously, Xu et al. [72] used a mild defect-etching reaction to produce in-plane holey graphene oxide (HGO), in which GO and H_2O_2 were mixed and reacted at 100°C for 4 h (Figure 2b). The transmission electron microscopy (TEM) image revealed numerous planar pores of several nanometers on the HGO surface (Figure 2c). And nitrogen adsorption–desorption tests demonstrated a much higher SSA ($\sim 430 \text{ m}^2/\text{g}$) compared to GO ($\sim 180 \text{ m}^2/\text{g}$), along with a prominent size distribution in 2–3 nm. Considering the significantly improved SSAs and ion diffusion dynamics compared to the non-porous counterparts, the HGO could serve as binder-free supercapacitor electrodes with ultra-high electrochemical performances in various electrolytes. With the poly (vinyl alcohol) (PVA)- H_2SO_4 gel electrolyte, the HGO-based SCs demonstrated a specific capacitance of 201 F/g at 1 A/g, exceptional flexibility even at a bending radius of ~ 2 mm, and an outstanding cycling stability of $\sim 90\%$ of retention after 20,000 cycles under the bending state (Figure 2d–g).

In summary, the pore structure of disordered mesoporous graphene obtained using various strategies is randomly distributed and uncontrollable. And the generated structural defects limit the repetitive synthesis and mechanism study of GMNs for SCs. Therefore, the in-plane mesoporous graphene with ordered mesopores may be more meaningful and promising.

2.2. Ordered Mesoporous Graphene

Ordered mesoporous graphene possesses uniform pore sizes and orderly arranged mesopores in the basal plane. In order to accurately customize the pore structure, various template strategies have been developed, mainly involving the construction of mesopores inside graphene nanosheets using rigid nanoparticles or flexible molecules as the hard or soft templates [40,57,68]. For instance, Fang et al. [73] reported a low-concentration micelle

close-packing assembly strategy to controllably synthesize ordered mesoporous graphene. As shown in Figure 3a, the phenolic resin molecules interacted with triblock copolymer Pluronic F127 templates to form spherical micelles, and then the subunits were assembled in a close-packed manner through hydrothermal treatment to gain two-dimensional (2D) ordered mesoporous carbon nanosheets. Thereinto, anodized alumina (AAO) films were used as substrates, providing a large surface area for 2D carbon production. Further, the mesoporous carbon nanosheets were converted to mesoporous graphene through carbonization at 700 °C. Notably, the obtained mesoporous graphene displayed tens of microns of average length and 400–500 nm of width, as well as a uniform mesopore size of ~9 nm (Figure 3b). Owing to the high SSA (~283 m²/g) and ordered mesopores, the mesoporous graphene showed an outstanding lithium-ion storage capacity and cycling performance. However, their SC application was not involved.

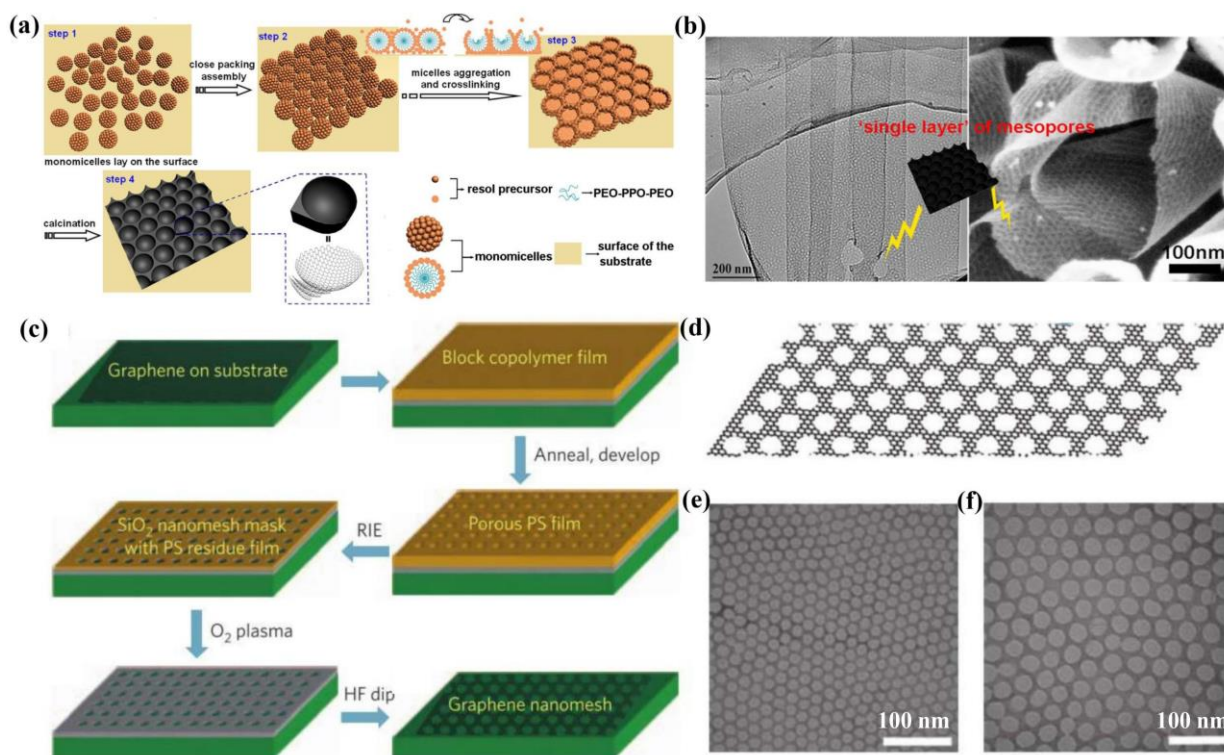


Figure 3. (a) Schematic of the preparation, and (b) TEM and SEM images of the ordered mesoporous graphene [73]. (c) Schematic of the fabrication of ordered GNM through block copolymer photolithography, (d) schematic of the structure, and (e,f) TEM images of GNM with 39 nm periodicity and 7.1 nm neck width [63].

In addition, Bai et al. [63] successfully prepared an ordered graphene nanomesh (GNM) with regulable periodicity and neck width (5–20 nm) using block copolymer photolithography. Specifically, graphene was employed as a 2D precursor, SiO_x film served as a protective layer and subsequent hard mask, and polystyrene block-methyl methacrylate (PS-*b*-MMA) block copolymer worked as the sacrificial template (Figure 3c). By etching away the underlying SiO_x, the individual GNM could be stripped off (Figure 3d). As shown in Figure 3e,f, the GNM showed uniform mesopores of 39 nm and an average neck width of 7.1 nm. Although it is inherently scalable for manufacturing continuous semiconductor GNM films, this method is limited by high-cost, low-yield, and dangerous conditions because of the usage of CHF₃ plasmon-based reactive ion etching (RIE) and O₂ plasma etching.

To sum up, the controllable fabrication of ordered mesoporous graphene is difficult and their SC applications is undeveloped at present. Therefore, the exploitation of novel

preparation methods and the investigation of the structure–activity relationship of ordered mesoporous graphene for SCs are innovative and urgently needed.

3. Sandwich-like Graphene-Based Mesoporous Heterostructures

As a kind of 2D nanocomposite, the sandwich-like GMNs are obtained by in situ patterning the mesoporous functional layer on both sides of the graphene substrate. It is hoped to greatly reduce the stacking of graphene nanosheets, extend the physicochemical properties of materials, and meet the multifunctional requirements of devices (e.g., SCs). Up to now, various sandwich-like GMNs have been developed, including mesoporous carbon/graphene, mesoporous heteroatom-doped carbon/graphene, mesoporous conducting polymer/graphene, mesoporous metal oxide/graphene, and so on [41,74–76].

3.1. Mesoporous Carbon/Graphene

Due to their excellent conductivity, superior electrochemical stability, cheap price, and environmental friendliness, carbon materials are recognized as one of the most common electrode materials of SCs [77–79]. Thus, by coupling the carbon component, mesopore structure, and graphene substrate, the resulting mesoporous carbon/graphene displays a high specific capacitance, outstanding rate performance, and good cycling stability. For example, Yang et al. [80] proposed a bottom-up method for the mass production of sandwich-like graphene-based mesoporous silica (GM-silica) nanosheets, where the graphene nanosheet was completely separated by the mesoporous silica layer. Then, GM-silica nanosheets could be used as a template to produce graphene-based mesoporous carbon and graphene-based mesoporous Co_3O_4 . As shown in Figure 4a–d, the pore size of the prepared graphene-based mesoporous carbon nanosheets was ~ 2 nm, the thickness was ~ 28 nm, and their SSA was up to $980 \text{ m}^2/\text{g}$. Further, the graphene-based mesoporous carbon as the active electrode presented good electrochemical performance for lithium-ion storage, while its SC application was not reported.

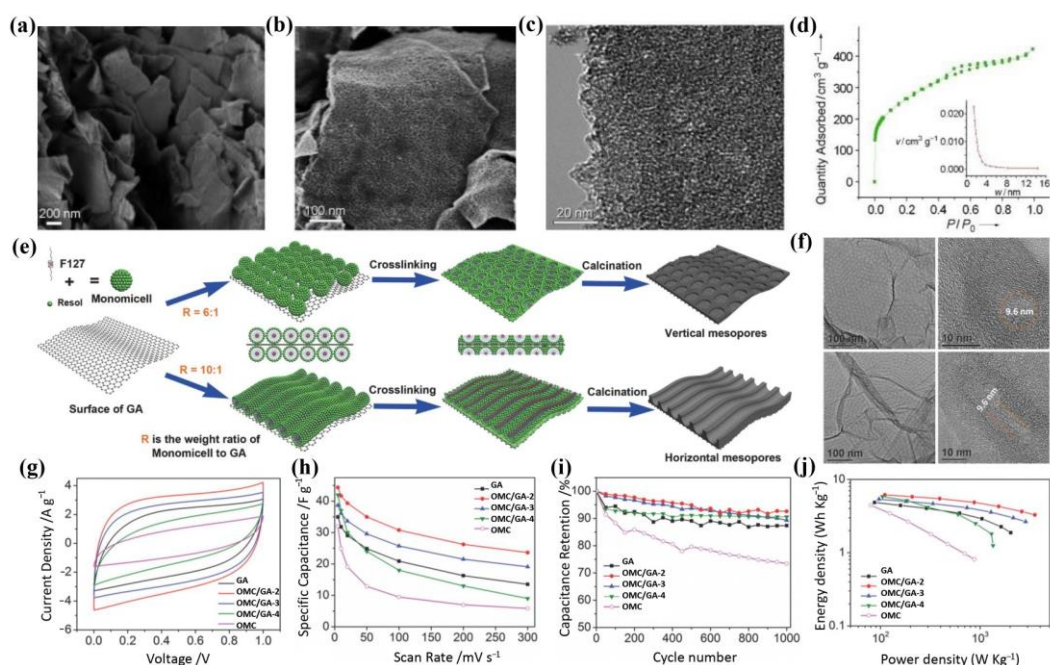


Figure 4. (a,b) SEM images, (c) TEM image, and (d) nitrogen adsorption/desorption isotherm of graphene-based mesoporous carbon [80]. (e) Schematic of the preparation; (f) TEM images of OMC/GA with different mesopore orientations; (g) CV curves; (h) specific capacitance versus current density; (i) cycling stability; and (j) Ragone plots of SCs based on OMC, GA, and different OMC/GA [81].

In addition, Liu et al. [81] firstly reported the interface-induced co-assembly of ordered mesoporous carbon/graphene aerogel (OMC/GA) composites for SCs, where the GA, F127, and resols were used as the macroporous substrate, mesopore template, and carbon source, respectively (Figure 4e). Prominently, the obtained OMC/GA was constituted by a network of highly ordered mesoporous carbon (~9.6 nm) on interconnected macroporous graphene (Figure 4f). During co-assembly, the weight ratio of resol-F127 micelles to GA could easily change the orientation of the mesopore structure (perpendicular or horizontal to the GA surface), which also had a great influence on their electrochemical behavior. As shown in Figure 4g,h, the OMC/GA with vertical mesopore (OMC/GA-2)-based all-solid-state SCs exhibited a superior specific capacitance of 44.3 F/g at 5 mV/s, rate capability of 23.6 F/g at 300 mV/s, cycling stability of 7.4% loss after 1000 cycles, energy density of ~6.2 Wh/kg, and power density of ~3545 Wh/kg compared to other counterparts. Therefore, this method provided a promising platform for the development of mesoporous graphene composites with controllable mesopores, and they were expected to show wide applications in SCs, batteries, sensors, and catalysis.

3.2. Mesoporous Heteroatom-Doped Carbon/Graphene

It is well known that the introduction of heteroatoms (e.g., N, O, S, and P) into mesoporous carbon/graphene can improve its wettability in electrolytes, change the electronic structure and physicochemical properties, and thus exhibit pseudocapacitance for SC application [82–85]. In recent years, nitrogen-doping has been deemed to be one of the most widely used strategies to enhance the electrochemical performance of mesoporous carbon/graphene. For instance, our group controllably synthesized a series of mesoporous nitrogen-doped carbon/graphene nanosheets (mNC/G) with SiO₂ nanospheres as a mesopore template and graphene as a 2D substrate (Figure 5a) [86]. The mNC/G nanosheets with varying mesopore sizes of 7 nm, 12 nm, and 22 nm were successfully achieved by changing the size of the SiO₂ template. As exhibited in Figure 5b, the mNC/G with 7 nm mesopores presented a specific capacitance of 267 F/g at 0.5 A/g, which was much higher than those of mNC/G with 12 nm mesopores (202 F/g) and 22 nm mesopores (157 F/g). This result was probably attributed to the smaller mesopores, larger SSAs, more active sites, and thus higher specific capacitance. Further, the mNC/G-based micro-supercapacitors (MSCs) showed a volumetric capacitance of 21.0 F/cm³ and a volume energy density of 1.9 mWh/cm³, exceeding most of the reported graphene-based MSCs (Figure 5c).

Apart from the hard template of SiO₂ nanospheres, soft templates (e.g., micelles of surfactants or block copolymer) can also be used to prepare nitrogen-doped mesoporous carbon/graphene. For example, Zhang et al. [87] synthesized 2D GO@nitrogen-doped mesoporous carbon (GO@NMC) using a simple, multistage, and self-assembled strategy, where poly-diaminopyridine (PDAP) acted as both carbon and nitrogen precursors, the polystyrene-*b*-polyethylene oxide (PS-*b*-PEO) block copolymer served as mesopore templates, and GO worked as a structural guide for 2D morphology (Figure 5d). After high-temperature carbonization (700 °C), GO@NMC with a mesopore range of 8–25 nm and N content of up to 19 wt% was produced (Figure 5e). Using it as an active electrode material, the resulting GO@NMC-based SCs displayed a specific capacitance of ~256 F/g at 0.2 A/g and excellent cycling stability for 5000 cycles (Figure 5f,g). In addition, the triblock copolymer of Pluronic P123 was used as a soft template to prepare mesoporous nitrogen-doped carbon/reduced GO (mNC/rGO) nanosheets. Specifically, P123 firstly formed columnar micelles in water, and then the micelles and dopamine (DA) molecules co-assembled on the GO surface through hydrogen bonding and electrostatic interactions. Through polymerization of DA, removal of P123, and hydrothermal treatment, mesoporous polydopamine/rGO (mPDA/rGO) was successfully obtained, and then mNC/rGO was received after further high-temperature carbonization treatment (Figure 5h). From transmission electron microscopy (TEM), it could be seen that the curved cylindrical mesopores were evenly distributed on rGO nanosheets (Figure 5i). Furthermore, with the mPDA/rGO positive electrode and mNC/rGO negative electrode, the prepared lithium-ion capacitor

(LiC) exhibited excellent electrochemical performance, e.g., an energy density of 208 Wh/kg at a power density of 176 W/kg, which was the highest value of the recently reported PDA-based LICs (Figure 5j).

In addition, polyatom-doped mesoporous carbon/graphene was developed and applied in SCs [38,88,89]. For instance, Xu et al. [38] prepared nitrogen–sulfur co-doped mesoporous carbon/graphene with a uniform mesopore structure (10 nm) using a 2D mesopore dual-template method (Figure 6a,b). Unluckily, the composite was not used in SCs, but as a carbon-based catalyst for oxygen reduction reaction (ORR). Moreover, Tan et al. [88] used GO as a 2D substrate, F127 as a soft template, and resin and phytic acid as organic precursors to synthesize phospho-nitrogen co-doped mesoporous carbon nanosheets (rGO@PN/C) (Figure 6c). Notably, the doping amount of nitrogen and phosphorus was 1.9 at% and 0.5 at%, the thickness was 27.8 nm, the mesopore diameter was ~ 14 nm, and the SSA was 1116.7 m^2/g , respectively. Meanwhile, TEM and high-angle annular dark-field scanning transmission electron microscopy (HAADF-STEM) confirmed that the introduction of the phosphorus element did not change the morphology of mesoporous nanosheets (Figure 6d,e). Owing to the high SSA, low thickness, rich mesopore structure, and phospho-nitrogen co-doping, the rGO@PN/C exhibited high activity and rapid mass transfer for ORR. Furthermore, Guo et al. [89] reported porous phospho-nitrogen co-doped carbon/graphene heterostructures (NPC/rGO) using metal–organic framework (MOF)-nanoparticles as a precursor through stepwise pyrolysis and phosphorylation process (Figure 6f). In the NaCl aqueous electrolyte, the NPC/rGO presented the highest specific capacitance of 228 F/g at 5 mV/s compared to contrast samples (Figure 6g). Therefore, polyatom-doping of mesoporous carbon/graphene may exhibit better electrochemical properties compared with single heteroatom-doping, and their applications in SCs will be an important research direction in the future.

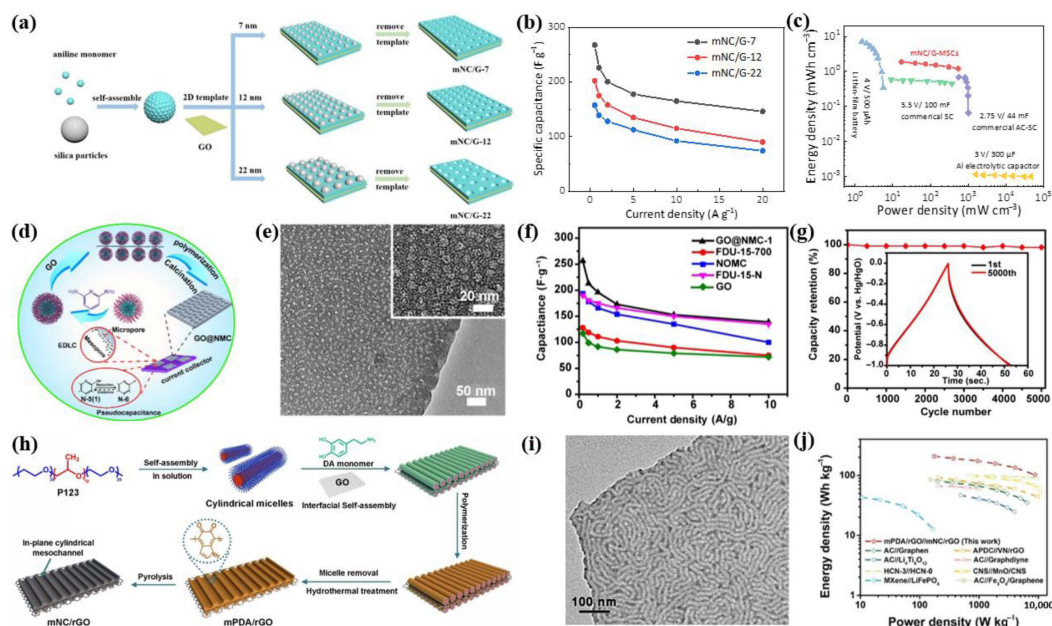


Figure 5. (a) Schematic of the synthesis and (b) specific capacitance versus current density of mNC/G. (c) Ragone plot of mNC/G-MSCs [86]. (d) Schematic of the fabrication, (e) TEM images, (f) specific capacitance versus current density, and (g) cycling stability of GO@NMC [87]. (h) Diagram of the synthesis process and (i) TEM image of mNC/rGO. (j) Ragone plots of the mPDA/rGO//mNC/rGO LIC with different reported LICs [90].

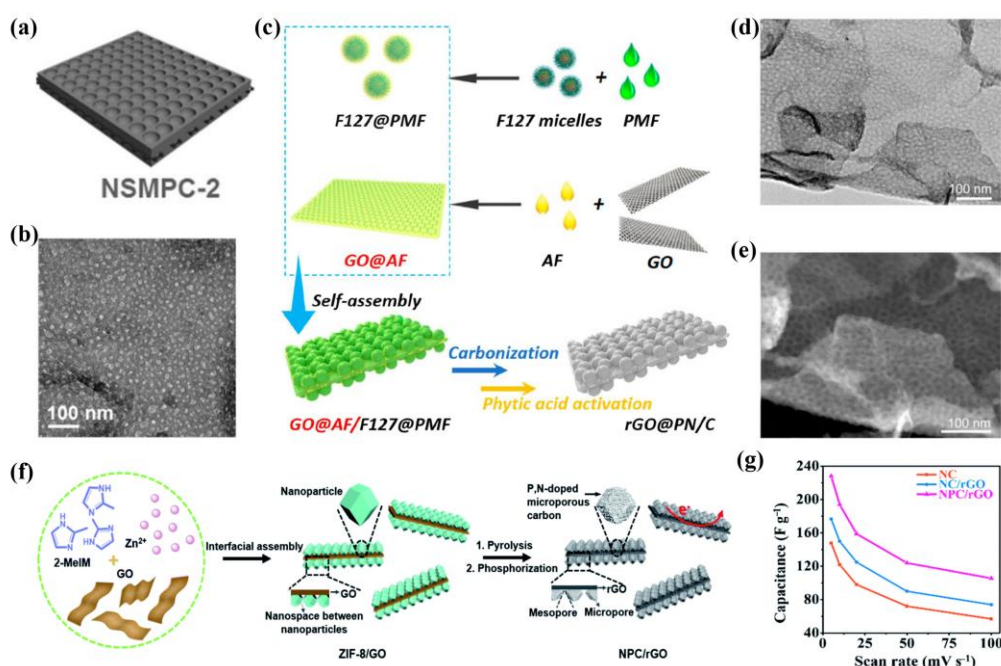


Figure 6. (a) Schematic diagram and (b) TEM image of NSMPC [38]. (c) Illustration of the fabrication, (d) TEM image, and (e) SEM image of rGO@PN/C [88]. (f) Schematic for the preparation of NPC/rGO, and (g) specific capacitances of NPC/rGO and other samples [89].

3.3. Mesoporous Conducting Polymer/Graphene

The conducting polymer refers to the highly conductive copolymer, such as polypyrrole (PPy) [45,91–93] and polyaniline (PANi) [94–96]. In order to overcome the high volume expansion/contraction during the charge/discharge process, the mesoporous conducting polymer is usually in situ grown on graphene to form GMNs with a sandwich-like structure. For example, Liu et al. [97] employed the spherical micelles of an amphiphilic block polymer (PS-*b*-PEO) as soft mesopore templates to fabricate mesoporous conducting polymer-GO nanosheets (Figure 7a). The TEM and SEM characterizations confirmed the highly regular and uniform mesopore structure for mesoporous PPy-GO (mPPy@GO, Figure 7b,c). Furthermore, mPPy@GO with 19.3 nm mesopores revealed a high specific capacitance (300 F/g at 1 mV/s) and excellent cycling stability (~99% retention after 5000 cycles), as shown in Figure 7d,e. And the mPPy@GO-based MSCs displayed an areal capacitance of 19 mF/cm² and high rate capability up to 100 V/s. For another example, Mai's group demonstrated the general preparation of graphene-based 2D mesoporous polymer nanosheets using pyrrole, aniline, and dopamine as monomers [31]. Specifically, the cylindrical micelles of P123 block copolymer were used as the mesopore templates, which interacted with the pyrrole, aniline, or dopamine monomer and GO substrate through hydrogen bonding. After the polymerization of monomers, removal of P123 templates, and hydrothermal treatment, the mesoporous conducting polymer/rGO nanosheets including mesoporous PPy/rGO (mPPy/rGO), mesoporous PANi/rGO, and mesoporous polydopamine/rGO were obtained (Figure 7f). Notably, the SEM and TEM images showed a clear mesopore structure with 11 nm for mPPy/rGO (Figure 7g,h). Further, the mPPy/rGO-based MSCs exhibited an impressive electrochemical performance, e.g., volumetric capacitance of 102 F/cm³ and areal capacitance of 81 mF/cm² at 1 mV/s (Figure 7i). In addition, their energy density (2.3 mWh/cm³) was higher than the commercial energy storage devices and some reported MSCs, proving the good application prospects of the mesoporous conducting polymer/graphene and corresponding MSCs (Figure 7j).

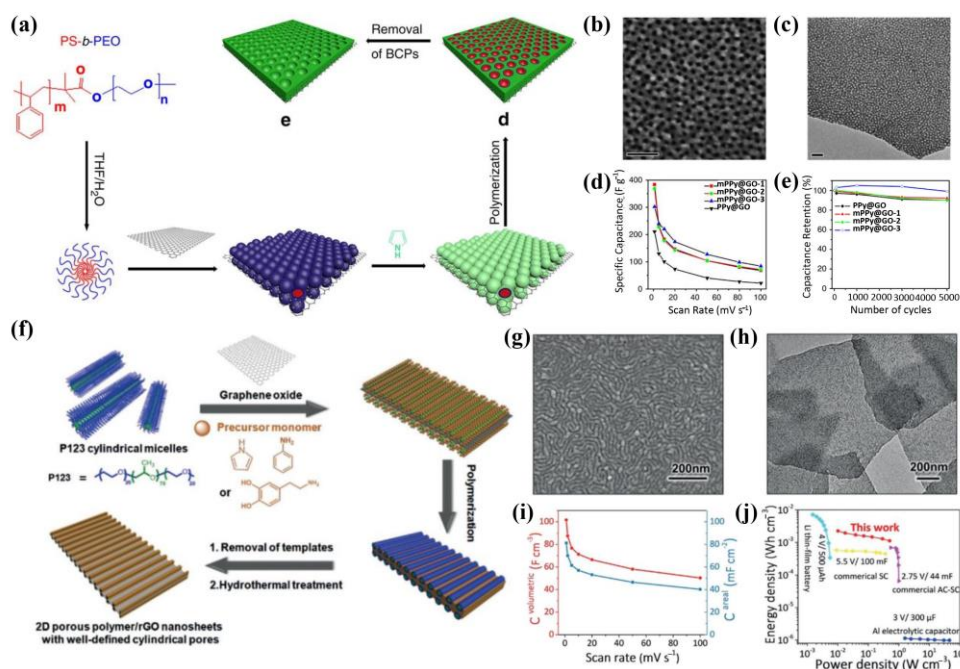


Figure 7. (a) Schematic of the preparation of mesoporous conducting polymer-GO nanosheets, (b) SEM image, (c) TEM image, (d) specific capacitance versus current density, and (e) cycling stability of mPPy@GO with different mesopore sizes [97]. (f) Schematic of the preparation of mesoporous polymer/rGO nanosheets, (g) SEM image, and (h) TEM image of mPPy@rGO. (i) Areal capacitance and volumetric capacitance, and (j) Ragone plots of mPPy/rGO-based MSCs and some commercial energy storage devices [31].

Considering that the single mesopore structure cannot satisfy the multi-functional demand for material design and device application, Qin et al. [75] developed ordered dual-mesoporous polypyrrole/graphene (DM-PG) using a soft and hard dual-mesopore template strategy. Significantly, the sandwich-like DM-PG possessed well-defined small and large mesopore arrays (~ 7 nm and 18 nm) on both sides of graphene, which yielded a larger specific capacitance of 376 F/g at 1 mV/s and a higher NH_3 response compared with single mesoporous and non-mesoporous samples (Figure 8a–d). Using the PVA- H_2SO_4 gel electrolyte, the resulting MSCs presented an areal capacitance and volumetric capacitance of 38 mF/cm² and 110 F/cm³, respectively (Figure 8e). The Ragone plot of DM-PG-based MSCs is displayed in Figure 8f, revealing a superior volumetric energy density (2.5 mWh/cm³). More importantly, DM-PG nanosheets could be used as bifunctional active materials of an MSC and NH_3 sensor for the simultaneous construction of a planar MSC-sensor integrated system with excellent compatibility and good performance (Figure 8g).

Furthermore, phosphomolybdate (POM) redox molecules can be introduced into mesoporous conducting polymer/graphene to further improve the electrochemical performance of electrode materials and the corresponding SCs [98,99]. From this, Wu's group successfully prepared mesoporous PPy/graphene nanosheets with redox POM anchoring (mPPy@rGO-POM) using a soft template method for planar MSCs with enhanced volumetric capacitance [74]. Firstly, vermicular mesoporous mPPy@GO nanosheets were synthesized using P123 block copolymer as the mesopore template. After POM impregnation and the hydrothermal process, an mPPy@rGO-POM with low thickness (~ 3 nm), large SSA (142 m²/g), abundant mesopore structure, and uniform POM loading was obtained (Figure 8h,i). Further, the mPPy@rGO-POM-based MSCs presented a high areal capacitance of 115 mF/cm² and volumetric capacitance of 137 F/cm³, as well as an outstanding energy density of 4.8 mWh/cm³ and power density of 645.1 mW/cm³ (Figure 8j,k). This strategy was expected to open up many possibilities for designing high-performance GMNs and building next-generation, flexible energy storage devices.

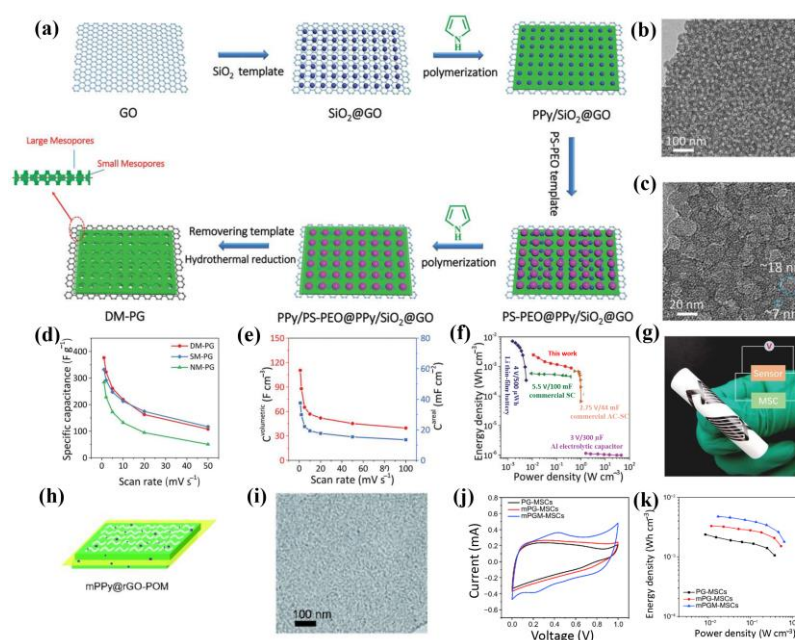


Figure 8. (a) Schematic of the synthesis and (b,c) TEM images of DM-PG, (d) specific capacitance comparison of DM-PG and its counterparts, (e) volumetric and areal capacitances, (f) Ragone plot of DM-PG-based MSCs with commercial energy storage systems, and (g) DM-PG-based planar MSC-sensor-integrated system [75]. (h) Schematic diagram, (i) TEM image of mPPy@rGO-POM, (j) CV curves, and (k) Ragone plot of mPPy@rGO-POM-based MSCs [74].

3.4. Mesoporous Metal Oxide/Graphene

As active electrode materials, metal oxides store charge through surface and near-surface Faraday oxidation/reduction reactions, which can generate a larger pseudocapacitance than double-layer capacitance [100–103]. On account of their poor conductivity and high volume changes in the charge/discharge process, metal oxides can be combined with the 2D graphene and mesopore structure to fabricate mesoporous metal oxide/graphene to enhance their electrochemical performance. For instance, Yang et al. [104] prepared a graphene-based mesoporous SnO_2 composite (defined as G-M- SnO_2) with cetyltrimethylammonium bromide (CTAB) as the structure-guiding agent. Obviously, the SnO_2 grew uniformly on the surface of graphene, and the mesopore size was about 3 nm (Figure 9a–c). However, the G-M- SnO_2 was applied to batteries but not SCs. Further, Lan et al. [105] reported a confined interfacial micelle assembly technique for the controllable synthesis of ordered mesoporous TiO_2 on different substrates (e.g., SiO_2 , carbon, polymer, metal oxide, and metal sulfide) for the first time. Using Pluronic F127 as the mesopore template, GO as the substrate, and glycerol as the confined solvent, highly ordered m TiO_2 /GO nanosheets were successfully prepared. The TEM characterization exhibited a uniform mesopore structure with 9.5 nm (Figure 9d,e). Notably, this method had a certain universality for most 2D materials to construct mesoporous TiO_2 -based nanosheets. In addition, Tong et al. [106] prepared the mesoporous Nb_2O_5 /graphene/mesoporous Nb_2O_5 (G@m Nb_2O_5) nanosheets through a simple two-step hydrolysis technique. As shown in Figure 9f, the TEM images verified the uniform coverage of Nb_2O_5 nanoparticles on graphene. The nitrogen physisorption measurements further confirmed the existence of 1–4 nm mesopores (Figure 9g). Then, the electrochemical behavior of G@m Nb_2O_5 was investigated using a sodium-ion half-cell, in which the capacities at 50 and 2000 mA/g were 293 and 125 mAh/g, respectively (Figure 9h,i). With an activated carbon cathode and G@m Nb_2O_5 anode, a full sodium-ion hybrid SC was successfully fabricated. It displayed an outstanding energy density of 56.1 Wh/kg at 120 W/kg and a good cycling stability of ~89% of retention for 800 cycles (Figure 9j,k). These results demonstrated the feasibility of G@m Nb_2O_5 nanosheets for high-energy and high-power sodium-ion hybrid devices.

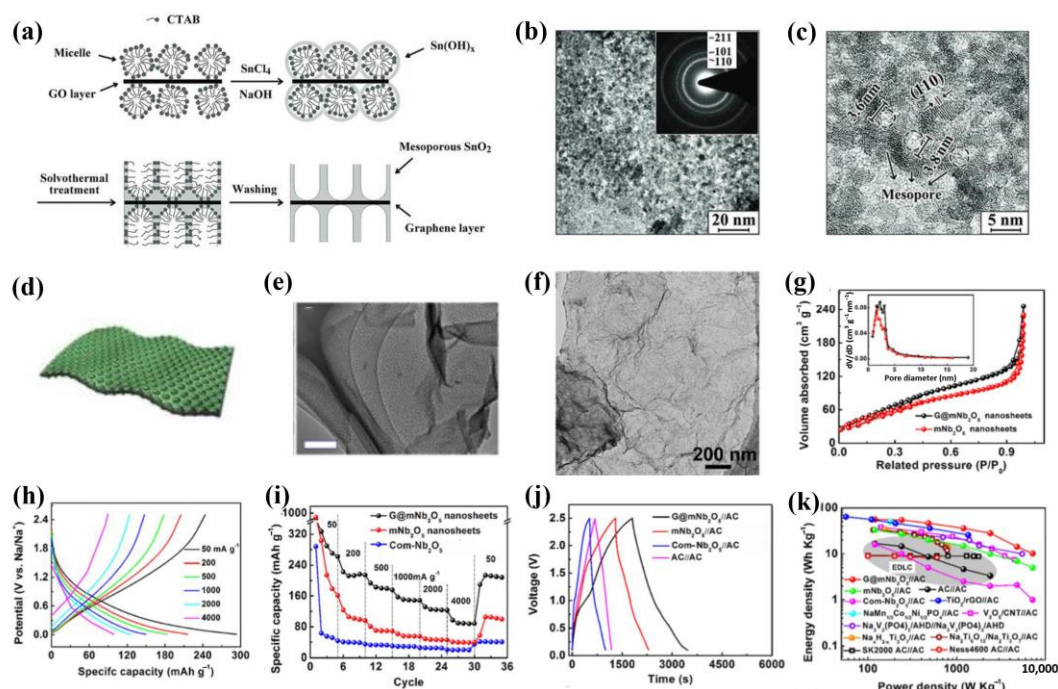


Figure 9. (a) Schematic for the formation and (b,c) TEM images of G-M-SnO₂ [104]. (d) Schematic diagram of the structure and (e) TEM image of mTiO₂/GO [105]. (f) TEM image, (g) nitrogen adsorption/desorption isotherms, (h) GCD profiles, (i) rate performance of G@mNb₂O₅ nanosheets, (j) GCD profiles at 0.05 A/g, and (k) Ragone plots of G@mNb₂O₅//AC device with other representative sodium-ion hybrid SCs [106].

4. Summary and Perspective

In this review, the chemical synthesis and SC applications of GMNs (including in-plane mesoporous graphene and sandwich-like mesoporous graphene-based heterostructures) are summarized in detail. Specifically, physical/chemical etching and template methods are the primary synthesis strategies for disordered and ordered mesoporous graphene, respectively. The in-plane mesopores enable mesoporous graphene with an increased SSA and rapid ion transport, as well as SCs with an enhanced specific capacitance and rate performance. Sandwich-like mesoporous graphene heterostructures with varying compositions (e.g., carbon/graphene, heteroatom-doped carbon/graphene, conducting polymer/graphene, and metal oxide/graphene) have been produced using various template methods. They can greatly restrain the restacking of graphene nanosheets and improve the electrochemical performance of materials and corresponding SCs. However, there are still some unresolved challenges in GMNs for SCs.

(1) Obviously, the reported GMNs are limited to mesoporous graphene, mesoporous carbon/graphene, heteroatom-doped carbon/graphene, conducting polymer/graphene, and metal oxide/graphene so far. Thus, the development of new GMNs, such as mesoporous metal sulfides/carbides/nitrides, metals, metal–organic frameworks, and covalent organic frameworks/graphene heterostructures, is vital and promising, which will generate special physicochemical properties for SC applications. (2) From the view of synthetic strategies, the mesopore template method is the most common strategy used to controllably prepare GMNs. However, the complicated steps and harsh reaction conditions impede their large-scale production. To meet the industrial or commercial demands, simpler and more efficient synthesis technologies are demanded for GMNs. (3) At present, there are few studies on the application of GMNs in SCs, and some research only reported the synthesis of GMNs but did not involve their SC applications [38,70,73]. So, the investigation of SC applications and the summary of performance parameters for GMNs are crucial in the future. (4) The exploration of the structure–activity relationship of GMNs is still in the initial stage, and only a few reports have discussed the effects of pore size and sheet thickness

on their electrochemical performance [86,97]. Therefore, it is necessary to systematically study the role of the composition, SSA, pore shape, pore size, or thickness of GMNs in SC applications, and the in situ characterization may provide an important platform.

In summary, the structural advantages, synthesis methods, and SC applications of GMNs have been thoroughly discussed, revealing their promising future and existing challenges. Although GNMNs are still in their infancy, they have opened up a new space in the field of materials science, and their commercialization can be expected soon after surmounting the above unsolved problems.

Author Contributions: Conceptualization, L.Z. and J.Q.; methodology, W.B.; software, H.Z.; validation, W.B., H.Z. and G.Y.; formal analysis, W.B.; investigation, H.Z.; resources, G.Y.; data curation, W.B.; writing—original draft preparation, W.B., H.Z. and G.Y.; writing—review and editing, L.Z. and J.Q.; visualization, G.Y.; supervision, L.Z. and J.Q.; project administration, L.Z. and J.Q.; funding acquisition, J.Q. All authors have read and agreed to the published version of the manuscript.

Funding: This research was funded by the National Natural Science Foundation of China, grant number 22109040, the Top-Notch Talent Program of Henan Agricultural University, grant number 30500947, and the fund of the State Key Laboratory of Catalysis in DICP, grant number N–22–15.

Data Availability Statement: Data that support the findings of this study are contained within the article.

Acknowledgments: The authors acknowledge the National Natural Science Foundation of China (Grant 22109040), the Top-Notch Talent Program of Henan Agricultural University (Grant 30500947), and the fund of the State Key Laboratory of Catalysis in DICP (Grant N–22–15).

Conflicts of Interest: The authors declare no conflict of interest.

References

1. Chu, S.; Majumdar, A. Opportunities and challenges for a sustainable energy future. *Nature* **2012**, *488*, 294–303. [[CrossRef](#)] [[PubMed](#)]
2. Chaudhari, N.K.; Jin, H.; Kim, B.; San Baek, D.; Joo, S.H.; Lee, K. MXene: An emerging two-dimensional material for future energy conversion and storage applications. *J. Mater. Chem. A* **2017**, *5*, 24564–24579. [[CrossRef](#)]
3. Dunn, B.; Kamath, H.; Tarascon, J.-M. Electrical energy storage for the grid: A battery of choices. *Science* **2011**, *334*, 928–935. [[CrossRef](#)] [[PubMed](#)]
4. Lukatskaya, M.R.; Dunn, B.; Gogotsi, Y. Multidimensional materials and device architectures for future hybrid energy storage. *Nat. Commun.* **2016**, *7*, 12647. [[CrossRef](#)]
5. Liu, C.; Li, F.; Ma, L.P.; Cheng, H. Advanced materials for energy storage. *Adv. Mater.* **2010**, *22*, E28–E62. [[CrossRef](#)]
6. Mahlia, T.M.I.; Saktisahdan, T.J.; Jannifar, A.; Hasan, M.H.; Matseelar, H.S.C. A review of available methods and development on energy storage; technology update. *Renew. Sustain. Energ. Rev.* **2014**, *33*, 532–545. [[CrossRef](#)]
7. Zhang, P.; Wang, F.; Yu, M.; Zhuang, X.; Feng, X. Two-dimensional materials for miniaturized energy storage devices: From individual devices to smart integrated systems. *Chem. Soc. Rev.* **2018**, *47*, 7426–7451. [[CrossRef](#)]
8. Wang, J.; Li, F.; Zhu, F.; Schmidt, O.G. Recent progress in micro-supercapacitor design, integration, and functionalization. *Small Methods* **2018**, *3*, 1800367. [[CrossRef](#)]
9. Zhong, C.; Deng, Y.; Hu, W.; Qiao, J.; Zhang, L.; Zhang, J. A review of electrolyte materials and compositions for electrochemical supercapacitors. *Chem. Soc. Rev.* **2015**, *44*, 7484–7539. [[CrossRef](#)]
10. Yang, J.; Bao, W.; Jaumaux, P.; Zhang, S.; Wang, C.; Wang, G. MXene-based composites: Synthesis and applications in rechargeable batteries and supercapacitors. *Adv. Mater. Interfaces* **2019**, *6*, 1802004. [[CrossRef](#)]
11. Ma, R.; Chen, Z.; Zhao, D.; Zhang, X.; Zhuo, J.; Yin, Y.; Wang, X.; Yang, G.; Yi, F. Ti₃C₂T_x MXene for electrode materials of supercapacitors. *J. Mater. Chem. A* **2021**, *9*, 11501–11529. [[CrossRef](#)]
12. Hu, M.; Zhang, H.; Hu, T.; Fan, B.; Wang, X.; Li, Z. Emerging 2D MXenes for supercapacitors: Status, challenges and prospects. *Chem. Soc. Rev.* **2020**, *49*, 6666–6693. [[CrossRef](#)] [[PubMed](#)]
13. Huang, S.; Zhu, X.; Sarkar, S.; Zhao, Y. Challenges and opportunities for supercapacitors. *APL Mater.* **2019**, *7*, 100901. [[CrossRef](#)]
14. Amiri, A.; Bruno, A.; Polycarpou, A.A. Configuration-dependent stretchable all-solid-state supercapacitors and hybrid supercapacitors. *Carbon Energy* **2023**, *5*, e320. [[CrossRef](#)]
15. Zhan, C.; Zhang, P.; Dai, S.; Jiang, D. Boron supercapacitors. *ACS Energy Lett.* **2016**, *1*, 1241–1246. [[CrossRef](#)]
16. Yang, L.; Guo, X.; Jin, Z.; Guo, W.; Duan, G.; Liu, X.; Li, Y. Emergence of melanin-inspired supercapacitors. *Nano Today* **2021**, *37*, 101075. [[CrossRef](#)]
17. Libich, J.; Máca, J.; Vondrák, J.; Čech, O.; Sedlářková, M. Supercapacitors: Properties and applications. *J. Energy Storage* **2018**, *17*, 224–227. [[CrossRef](#)]

18. Zhang, L.; Yang, G.; Chen, Z.; Liu, D.; Wang, J.; Qian, Y.; Chen, C.; Liu, Y.; Wang, L.; Razal, J.; et al. MXene coupled with molybdenum dioxide nanoparticles as 2D-0D pseudocapacitive electrode for high performance flexible asymmetric micro-supercapacitors. *J. Mater.* **2020**, *6*, 138–144. [[CrossRef](#)]
19. Shao, Y.; El-Kady, M.F.; Sun, J.; Li, Y.; Zhang, Q.; Zhu, M.; Wang, H.; Dunn, B.; Kaner, R.B. Design and mechanisms of asymmetric supercapacitors. *Chem. Rev.* **2018**, *118*, 9233–9280. [[CrossRef](#)]
20. Wang, G.; Zhang, L.; Zhang, J. A review of electrode materials for electrochemical supercapacitors. *Chem. Soc. Rev.* **2012**, *41*, 797–828. [[CrossRef](#)]
21. Li, W.; Liu, J.; Zhao, D. Mesoporous materials for energy conversion and storage devices. *Nat. Rev. Mater.* **2016**, *6*, 1–17. [[CrossRef](#)]
22. Duan, L.; Wang, C.; Zhang, W.; Ma, B.; Deng, Y.; Li, W.; Zhao, D. Interfacial assembly and applications of functional mesoporous materials. *Chem. Rev.* **2021**, *121*, 14349–14442. [[CrossRef](#)] [[PubMed](#)]
23. Qin, J.; Yang, Z.; Xing, F.; Zhang, L.; Zhang, H.; Wu, Z. Two-dimensional mesoporous materials for energy storage and conversion: Current status, chemical synthesis and challenging perspectives. *Electrochem. Energy Rev.* **2023**, *6*, 9. [[CrossRef](#)]
24. Han Lyn, F.; Nur Hanani, Z.A. Graphene-based polymer nanocomposites in food packaging and factors affecting the behaviour of graphene-based materials: A review. *J. Nanopart. Res.* **2022**, *24*, 179. [[CrossRef](#)]
25. Jia, Y.; Zhang, J.; Kong, D.; Zhang, C.; Han, D.; Han, J.; Tao, Y.; Lv, W.; Yang, Q. Practical graphene technologies for electrochemical energy storage. *Adv. Funct. Mater.* **2022**, *32*, 2204272. [[CrossRef](#)]
26. Zheng, S.; Wu, Z.; Wang, S.; Xiao, H.; Zhou, F.; Sun, C.; Bao, X.; Cheng, H. Graphene-based materials for high-voltage and high-energy asymmetric supercapacitors. *Energy Storage Mater.* **2017**, *6*, 70–97. [[CrossRef](#)]
27. Zhu, C.; Han, L.; Hu, P.; Dong, S. In situ loading of well-dispersed gold nanoparticles on two-dimensional graphene oxide/SiO₂ composite nanosheets and their catalytic properties. *Nanoscale* **2012**, *4*, 1641–1646. [[CrossRef](#)]
28. Shi, X.; Wu, Z.; Qin, J.; Zheng, S.; Wang, S.; Zhou, F.; Sun, C.; Bao, X. Graphene-based linear tandem micro-supercapacitors with metal-free current collectors and high-voltage output. *Adv. Mater.* **2017**, *29*, 1703034. [[CrossRef](#)]
29. Wu, Z.; Yang, S.; Zhang, L.; Wagner, J.B.; Feng, X.; Müllen, K. Binder-free activated graphene compact films for all-solid-state micro-supercapacitors with high areal and volumetric capacitances. *Energy Storage Mater.* **2015**, *1*, 119–126. [[CrossRef](#)]
30. Xia, Z.; Mishukova, V.; Sollami Delekta, S.; Sun, J.; Sanchez, J.S.; Li, J.; Palermo, V. Selective deposition of metal oxide nanoflakes on graphene electrodes to obtain high-performance asymmetric micro-supercapacitors. *Nanoscale* **2021**, *13*, 3285–3294. [[CrossRef](#)]
31. Tian, H.; Qin, J.; Hou, D.; Li, Q.; Li, C.; Wu, Z.; Mai, Y. General interfacial self-assembly engineering for patterning two-dimensional polymers with cylindrical mesopores on graphene. *Angew. Chem. Int. Ed.* **2019**, *58*, 10173–10178. [[CrossRef](#)] [[PubMed](#)]
32. Lu, B.; Jin, X.; Han, Q.; Qu, L. Planar graphene-based microsupercapacitors. *Small* **2021**, *17*, 2006827. [[CrossRef](#)] [[PubMed](#)]
33. Qin, J.; Wang, S.; Zhou, F.; Das, P.; Zheng, S.; Sun, C.; Bao, X.; Wu, Z. 2D mesoporous MnO₂ nanosheets for high-energy asymmetric micro-supercapacitors in water-in-salt gel electrolyte. *Energy Storage Mater.* **2019**, *18*, 397–404. [[CrossRef](#)]
34. Peng, L.; Peng, H.; Xu, L.; Wang, B.; Lan, K.; Zhao, T.; Che, R.; Li, W.; Zhao, D. Anisotropic self-assembly of asymmetric mesoporous hemispheres with tunable pore structures at liquid-liquid interfaces. *J. Am. Chem. Soc.* **2022**, *144*, 15754–15763. [[CrossRef](#)]
35. Gou, Z.; Qu, H.; Liu, H.; Ma, Y.; Zong, L.; Li, B.; Xie, C.; Li, Z.; Li, W.; Wang, L. Coupling of N-doped mesoporous carbon and N-Ti₃C₂ in 2D sandwiched heterostructure for enhanced oxygen electroreduction. *Small* **2022**, *18*, 2106581. [[CrossRef](#)]
36. Allah, A.E.; Wang, J.; Kaneti, Y.V.; Li, T.; Farghali, A.A.; Khedr, M.H.; Nanjundan, A.K.; Ding, B.; Dou, H.; Zhang, X.; et al. Auto-programmed heteroarchitecturing: Self-assembling ordered mesoporous carbon between two-dimensional Ti₃C₂T_x MXene layers. *Nano Energy* **2019**, *65*, 103991. [[CrossRef](#)]
37. Wang, J.; Chang, Z.; Ding, B.; Li, T.; Yang, G.; Pang, Z.; Nakato, T.; Eguchi, M.; Kang, Y.M.; Na, J.; et al. Universal access to two-dimensional mesoporous heterostructures by micelle-directed interfacial assembly. *Angew. Chem. Int. Ed.* **2020**, *59*, 19570–19575. [[CrossRef](#)]
38. Xu, Z.; Li, L.; Chen, X.; Xiao, G. N,S-codoped mesoporous carbons derived from polymer micelle-based assemblies for the oxygen reduction reaction. *ACS Appl. Energy Mater.* **2021**, *4*, 1954–1961. [[CrossRef](#)]
39. Tan, H.; Tang, J.; Henzie, J.; Li, Y.; Xu, X.; Chen, T.; Wang, Z.; Wang, J.; Ide, Y.; Bando, Y.; et al. Assembly of hollow carbon nanospheres on graphene nanosheets and creation of iron–nitrogen-doped porous carbon for oxygen reduction. *ACS Nano* **2018**, *12*, 5674–5683. [[CrossRef](#)]
40. Wei, W.; Liang, H.; Parvez, K.; Zhuang, X.; Feng, X.; Mullen, K. Nitrogen-doped carbon nanosheets with size-defined mesopores as highly efficient metal-free catalyst for the oxygen reduction reaction. *Angew. Chem. Int. Ed.* **2014**, *126*, 1596–1600. [[CrossRef](#)]
41. Liu, Z.; Liu, S.; Dong, R.; Yang, S.; Lu, H.; Narita, A.; Feng, X.; Mullen, K. High power in-plane micro-supercapacitors based on mesoporous polyaniline patterned graphene. *Small* **2017**, *13*, 1603388. [[CrossRef](#)]
42. Li, H.; Fang, X.; Lv, F.; Yu, W.; Cheng, H.; Zhang, H. Controllable assembly of nitrogen-doped mesoporous carbon with different pore structures onto CNTs for excellent lithium storage. *Nano Res.* **2023**, *16*, 3879–3887. [[CrossRef](#)]
43. Li, K.; Wang, X.; Li, S.; Urbankowski, P.; Li, J.; Xu, Y.; Gogotsi, Y. An ultrafast conducting polymer@MXene positive electrode with high volumetric capacitance for advanced asymmetric supercapacitors. *Small* **2020**, *16*, 1906851. [[CrossRef](#)] [[PubMed](#)]
44. Liu, Z.; Xiong, H.; Luo, Y.; Zhang, L.; Hu, K.; Zhang, L.; Gao, Y.; Qiao, Z. Interface-induced self-assembly strategy toward 2D ordered mesoporous carbon/MXene heterostructures for high-performance supercapacitors. *ChemSusChem* **2021**, *14*, 4422–4430. [[CrossRef](#)] [[PubMed](#)]

45. Qian, Q.; Xu, X.; Guo, J.; Jonathan, P.; Xu, H.; Xiang, L.; Li, C.; Yamauchi, Y.; Mai, Y. Two-dimensional MXene-polymer heterostructure with ordered in-plane mesochannels for high-performance capacitive deionization. *Angew. Chem. Int. Ed.* **2021**, *60*, 26528–26534.
46. Ai, Y.; Li, W.; Zhao, D. 2D mesoporous materials. *Natl. Sci. Rev.* **2022**, *9*, nwab108. [[CrossRef](#)] [[PubMed](#)]
47. Liu, S.; Wang, F.; Dong, R.; Zhang, T.; Zhang, J.; Zhuang, X.; Mai, Y.; Feng, X. Dual-template synthesis of 2D mesoporous polypyrrole nanosheets with controlled pore size. *Adv. Mater.* **2016**, *28*, 8365–8370. [[CrossRef](#)] [[PubMed](#)]
48. Bonaccorso, F.; Colombo, L.; Yu, G.; Stoller, M.; Tozzini, V.; Ferrari, A.C.; Ruoff, R.S.; Pellegrini, V. Graphene, related two-dimensional crystals, and hybrid systems for energy conversion and storage. *Science* **2015**, *347*, 1246501. [[CrossRef](#)]
49. Kumar, R.; Sahoo, S.; Joanni, E.; Singh, R.K.; Maegawa, K.; Tan, W.K.; Kawamura, G.; Kar, K.K.; Matsuda, A. Heteroatom doped graphene engineering for energy storage and conversion. *Mater. Today* **2020**, *39*, 47–65. [[CrossRef](#)]
50. Zhao, X.; Jiaqiang, E.; Wu, G.; Deng, Y.; Han, D.; Zhang, B.; Zhang, Z. A review of studies using graphenes in energy conversion, energy storage and heat transfer development. *Energy Convers. Manag.* **2019**, *184*, 581–599. [[CrossRef](#)]
51. Zhou, F.; Huang, H.; Xiao, C.; Zheng, S.; Shi, X.; Qin, J.; Fu, Q.; Bao, X.; Feng, X.; Mullen, K.; et al. Electrochemically scalable production of fluorine-modified graphene for flexible and high-energy ionogel-based microsupercapacitors. *J. Am. Chem. Soc.* **2018**, *140*, 8198–8205. [[CrossRef](#)] [[PubMed](#)]
52. Zheng, S.; Wang, S.; Dong, Y.; Zhou, F.; Qin, J.; Wang, X.; Su, F.; Sun, C.; Wu, Z.; Cheng, H.; et al. All-solid-state planar sodium-ion microcapacitors with multidirectional fast ion diffusion pathways. *Adv. Sci.* **2019**, *6*, 1902147. [[CrossRef](#)] [[PubMed](#)]
53. Zhang, X.; Hou, L.; Ciesielski, A.; Samori, P. 2D materials beyond graphene for high-performance energy storage Applications. *Adv. Energy Mater.* **2016**, *6*, 1600671. [[CrossRef](#)]
54. Wang, Z.; Wang, W.; Coombs, N.; Soheilnia, N.; Geoffrey, A.O. Graphene oxide-periodic mesoporous silica sandwich nanocomposites with vertically oriented channels. *ACS Nano* **2010**, *4*, 7437–7450. [[CrossRef](#)]
55. Xu, Y.; Lin, Z.; Zhong, X.; Huang, X.; Weiss, N.O.; Huang, Y.; Duan, X. Holey graphene frameworks for highly efficient capacitive energy storage. *Nat. Commun.* **2014**, *5*, 4554. [[CrossRef](#)]
56. Wei, J.; Hu, Y.; Liang, Y.; Kong, B.; Zhang, J.; Song, J.; Bao, Q.; Simon, G.P.; Jiang, S.P.; Wang, H. Nitrogen-doped nanoporous carbon/graphene nano-sandwiches: Synthesis and application for efficient oxygen reduction. *Adv. Funct. Mater.* **2015**, *25*, 5768–5777. [[CrossRef](#)]
57. Wang, Q.; Yan, J.; Fan, Z.; Wei, T.; Zhang, M.; Jing, X. Mesoporous polyaniline film on ultra-thin graphene sheets for high performance supercapacitors. *J. Power Sources* **2014**, *247*, 197–203. [[CrossRef](#)]
58. Wang, N.; Tian, H.; Zhu, S.; Yan, D.; Mai, Y. Two-dimensional nitrogen-doped mesoporous carbon/graphene nanocomposites from the self-assembly of block copolymer micelles in solution. *Chin. J. Polym. Sci.* **2017**, *36*, 266–272. [[CrossRef](#)]
59. Sun, H.; Mei, L.; Liang, J.; Zhao, Z.; Lee, C.; Fei, H.; Ding, M.; Lau, J.; Li, M.; Wang, C.; et al. Three-dimensional holey-graphene/niobia composite architectures for ultrahigh-rate energy storage. *Science* **2017**, *356*, 599–604. [[CrossRef](#)]
60. Yadav, P.; Basu, A.; Suryawanshi, A.; Game, O.; Ogale, S. Highly stable laser-scribed flexible planar microsupercapacitor using mushroom derived carbon electrodes. *Adv. Mater. Interfaces* **2016**, *3*, 1600057. [[CrossRef](#)]
61. Shi, M.; Xiao, P.; Lang, J.; Yan, C.; Yan, X. Porous g-C₃N₄ and MXene dual-confined FeOOH quantum dots for superior energy storage in an ionic liquid. *Adv. Sci.* **2020**, *7*, 1901975. [[CrossRef](#)] [[PubMed](#)]
62. Guerra, V.L.P.; Valeš, V.; Mikšátko, J.; Plšek, J.; Drogowska-Horná, K.A.; Volochanskyi, O.; Kalbáč, M. The use of sample positioning to control defect creation by oxygen plasma in isotopically labelled bilayer graphene membranes. *RSC Adv.* **2021**, *11*, 10316–10322. [[CrossRef](#)] [[PubMed](#)]
63. Bai, J.; Zhong, X.; Jiang, S.; Huang, Y.; Duan, X. Graphene nanomesh. *Nat. Nanotechnol.* **2010**, *5*, 190–194. [[CrossRef](#)] [[PubMed](#)]
64. Wang, L.; Bi, X.; Yang, S. Partially single-crystalline mesoporous Nb₂O₅ nanosheets in between graphene for ultrafast sodium storage. *Adv. Mater.* **2016**, *28*, 7672–7679. [[CrossRef](#)]
65. Lou, Y.; Dourdain, S.; Rey, C.; Serruys, Y.; Simeone, D.; Mollard, N.; Deschanel, X. Structure evolution of mesoporous silica under heavy ion irradiations of intermediate energies. *Micropor. Mesopor. Mat.* **2017**, *251*, 146–154. [[CrossRef](#)]
66. Pan, D.; Yuan, P.; Zhao, L.; Liu, N.; Zhou, L.; Wei, G.; Zhang, J.; Ling, Y.; Fan, Y.; Wei, B.; et al. New understanding and simple approach to synthesize highly hydrothermally stable and ordered mesoporous materials. *Chem. Mater.* **2009**, *21*, 5413–5425. [[CrossRef](#)]
67. Nath, S.; Biswas, A.; Kour, P.P.; Sarma, L.S.; Sur, U.K.; Ankamwar, B.G. Synthesis of mesoporous nanocrystalline zirconia by surfactant-assisted hydrothermal approach. *J. Nanosci. Nanotechnol.* **2018**, *18*, 5390–5396. [[CrossRef](#)]
68. Xi, X.; Wu, D.; Han, L.; Yu, Y.; Su, Y.; Tang, W.; Liu, R. Highly uniform carbon sheets with orientation-adjustable ordered mesopores. *ACS Nano* **2018**, *12*, 5436–5444. [[CrossRef](#)]
69. Qian, M.; Xu, F.; Bi, H.; Lin, T.; Huang, F. Facile sol-gel method combined with chemical vapor deposition for mesoporous few-layer carbon. *Carbon* **2017**, *112*, 47–52. [[CrossRef](#)]
70. Gerung, H.; Brinker, C.J.; Brueck, S.R.J.; Han, S. In situ real-time monitoring of profile evolution during plasma etching of mesoporous low-dielectric-constant SiO₂. *J. Vac. Sci. Technol. A* **2005**, *23*, 347–354. [[CrossRef](#)]
71. Kim, H.-K.; Bak, S.-M.; Lee, S.W.; Kim, M.-S.; Park, B.; Lee, S.C.; Choi, Y.J.; Jun, S.; Han, J.; Nam, K.-W.; et al. Scalable fabrication of micron-scale graphene nanomeshes for high-performance supercapacitor applications. *Energy Environ. Sci.* **2016**, *9*, 1270–1281. [[CrossRef](#)]

72. Xu, Y.; Chen, C.Y.; Zhao, Z.; Lin, Z.; Lee, C.; Xu, X.; Wang, C.; Huang, Y.; Shakir, M.I.; Duan, X. Solution processable hholey graphene oxide and its derived macrostructures for high-performance supercapacitors. *Nano Lett.* **2015**, *15*, 4605–4610. [[CrossRef](#)] [[PubMed](#)]
73. Fang, Y.; Lv, Y.; Che, R.; Wu, H.; Zhang, X.; Gu, D.; Zheng, G.; Zhao, D. Two-dimensional mesoporous carbon nanosheets and their derived graphene nanosheets: Synthesis and efficient lithium ion storage. *J. Am. Chem. Soc.* **2013**, *135*, 1524–1530. [[CrossRef](#)] [[PubMed](#)]
74. Qin, J.; Zhou, F.; Xiao, H.; Ren, R.; Wu, Z. Mesoporous polypyrrole-based graphene nanosheets anchoring redox polyoxometalate for all-solid-state micro-supercapacitors with enhanced volumetric capacitance. *Sci. China Mater.* **2017**, *61*, 233–242. [[CrossRef](#)]
75. Qin, J.; Gao, J.; Shi, X.; Chang, J.; Dong, Y.; Zheng, S.; Wang, X.; Feng, L.; Wu, Z. Hierarchical ordered dual-mesoporous polypyrrole/graphene nanosheets as Bi-functional active materials for high-performance planar integrated system of micro-supercapacitor and gas sensor. *Adv. Funct. Mater.* **2020**, *30*, 1909756. [[CrossRef](#)]
76. Wu, Z.; Parvez, K.; Li, S.; Yang, S.; Liu, Z.; Liu, S.; Feng, X.; Mullen, K. Alternating stacked graphene-conducting polymer compact films with ultrahigh areal and volumetric capacitances for high-energy micro-supercapacitors. *Adv. Mater.* **2015**, *27*, 4054–4061. [[CrossRef](#)]
77. Yaroslavtsev, A.B.; Stenina, I.A. Carbon coating of electrode materials for lithium-ion batteries. *Surf. Innov.* **2021**, *9*, 92–110. [[CrossRef](#)]
78. Lu, H.; Zhao, X. Biomass-derived carbon electrode materials for supercapacitors. *Sustain. Energy Fuels* **2017**, *1*, 1265–1281. [[CrossRef](#)]
79. Li, Z.; Xu, K.; Pan, Y. Recent development of supercapacitor electrode based on carbon materials. *Nanotechnol. Rev.* **2019**, *8*, 35–49. [[CrossRef](#)]
80. Yang, S.; Feng, X.; Wang, L.; Tang, K.; Maier, J.; Mullen, K. Graphene-based nanosheets with a sandwich structure. *Angew. Chem. Int. Ed.* **2010**, *49*, 4795–4799. [[CrossRef](#)]
81. Liu, R.; Wan, L.; Liu, S.; Pan, L.; Wu, D.; Zhao, D. An interface-induced co-assembly approach towards ordered mesoporous carbon/graphene aerogel for high-performance supercapacitors. *Adv. Funct. Mater.* **2015**, *25*, 526–533. [[CrossRef](#)]
82. Ilnicka, A.; Skorupska, M.; Szkoda, M.; Zarach, Z.; Lukaszewicz, J.P. N-doped carbon materials as electrodes for highly stable supercapacitors. *Mater. Res. Lett.* **2022**, *11*, 213–221. [[CrossRef](#)]
83. Zhang, H.; Ling, Y.; Peng, Y.; Zhang, J.; Guan, S. Nitrogen-doped porous carbon materials derived from ionic liquids as electrode for supercapacitor. *Inorg. Chem. Commun.* **2020**, *115*, 107856. [[CrossRef](#)]
84. Wei, X.; Gou, H.; Mo, Z.; Guo, R.; Hu, R.; Wang, Y. Hierarchically structured nitrogen-doped carbon for advanced supercapacitor electrode materials. *Ionics* **2016**, *22*, 1197–1207. [[CrossRef](#)]
85. Sylla, N.F.; Ndiaye, N.M.; Ngom, B.D.; Mutuma, B.K.; Momodu, D.; Chaker, M.; Manyala, N. Ex-situ nitrogen-doped porous carbons as electrode materials for high performance supercapacitor. *J. Colloid Interface Sci.* **2020**, *569*, 332–345. [[CrossRef](#)]
86. Yang, Z.; Zhou, F.; Zhang, H.; Qin, J.; Wu, Z. Controllable synthesis of 2D mesoporous nitrogen-doped carbon/graphene nanosheets for high-performance micro-supercapacitors. *New Carbon Mater.* **2022**, *37*, 936–943. [[CrossRef](#)]
87. Zhang, L.; Wang, T.; Gao, T.; Xiong, H.; Zhang, R.; Liu, Z.; Song, S.; Dai, S.; Qiao, Z. Multistage self-assembly strategy: Designed synthesis of N-doped mesoporous carbon with high and controllable pyridine N content for ultrahigh surface-area-normalized capacitance. *CCS Chem.* **2021**, *3*, 870–881. [[CrossRef](#)]
88. Tan, H.; Zhao, Y.; Xia, W.; Zhao, J.; Xu, X.; Wood, K.; Sugahara, Y.; Yamauchi, Y.; Tang, J. Phosphorus and nitrogen-doped carbon nanosheets constructed with monolayered mesoporous architectures. *Chem. Mater.* **2020**, *32*, 4248–4256. [[CrossRef](#)]
89. Guo, J.; Xu, X.; Hill, J.P.; Wang, L.; Dang, J.; Kang, Y.; Li, Y.; Guan, W.; Yamauchi, Y. Graphene-carbon 2D heterostructures with hierarchically-porous P,N-doped layered architecture for capacitive deionization. *Chem. Sci* **2021**, *12*, 10334–10340. [[CrossRef](#)]
90. Jiang, S.; Xing, F.; Zhang, J.; Xiang, L.; Li, Q.; Xu, F.; Wu, Z.; Mai, Y. Two-dimensional redox polydopamine with in-plane cylindrical mesochannels on graphene for high-energy and high-power lithium-ion capacitors. *Chem. Eng. J.* **2023**, *452*, 139095. [[CrossRef](#)]
91. Niu, Q.; Guo, Y.; Gao, K.; Shao, Z. Polypyrrole/cellulose nanofiber aerogel as a supercapacitor electrode material. *RSC Adv.* **2016**, *6*, 109143–109149. [[CrossRef](#)]
92. Huang, Y.; Li, H.; Wang, Z.; Zhu, M.; Pei, Z.; Xue, Q.; Huang, Y.; Zhi, C. Nanostructured polypyrrole as a flexible electrode material of supercapacitor. *Nano Energy* **2016**, *22*, 422–438. [[CrossRef](#)]
93. Zhang, B.; Jiang, L.; Li, Y.; Cai, F.; Zhang, Q. Three-dimensional porous biocarbon wrapped by graphene and polypyrrole composite as electrode materials for supercapacitor. *J. Mater. Sci. Mater. Electron.* **2018**, *29*, 2568–2572.
94. Wang, H.; Lin, J.; Shen, Z. Polyaniline (PANi) based electrode materials for energy storage and conversion. *J. Sci. Adv. Mater. Devices* **2016**, *1*, 225–255. [[CrossRef](#)]
95. Li, J.; Xiao, D.; Ren, Y.; Liu, H.; Chen, Z.; Xiao, J. Bridging of adjacent graphene/polyaniline layers with polyaniline nanofibers for supercapacitor electrode materials. *Electrochim. Acta* **2019**, *300*, 193–201. [[CrossRef](#)]
96. Das, P.; Mondal, S.; Malik, S. Fully organic polyaniline nanotubes as electrode material for durable supercapacitor. *J. Energy Storage* **2021**, *39*, 102662. [[CrossRef](#)]
97. Liu, S.; Gordiichuk, P.; Wu, Z.; Liu, Z.; Wei, W.; Wagner, M.; Mohamed-Noriega, N.; Wu, D.; Mai, Y.; Herrmann, A.; et al. Patterning two-dimensional free-standing surfaces with mesoporous conducting polymers. *Nat. Commun.* **2015**, *6*, 8817. [[CrossRef](#)]
98. Thomas, J.; Kannan, K.R.; Ramanan, A. Nanostructured phosphomolybdates. *J. Chem. Sci.* **2008**, *120*, 529–536. [[CrossRef](#)]

99. Lira-Cantú, M.; Gómez-Romero, P. Electrochemical and chemical syntheses of the hybrid organic-inorganic electroactive material formed by phosphomolybdate and polyaniline. Application as anion-insertion electrodes. *Chem. Mater.* **1998**, *10*, 698–704. [[CrossRef](#)]
100. Yadav, S.; Devi, A. Recent advancements of metal oxides/nitrogen-doped graphene nanocomposites for supercapacitor electrode materials. *J. Energy Storage* **2020**, *30*, 101486. [[CrossRef](#)]
101. Wu, S.; Liu, J.; Wang, H.; Yan, H. A review of performance optimization of MOF-derived metal oxide as electrode materials for supercapacitors. *Int. J. Energy Res.* **2019**, *43*, 697–716. [[CrossRef](#)]
102. Cao, Y.; He, Y.; Gang, H.; Wu, B.; Yan, L.; Wei, D.; Wang, H. Stability study of transition metal oxide electrode materials. *J. Power Sources* **2023**, *560*, 232710. [[CrossRef](#)]
103. Mo, X.; Xu, G.; Kang, X.; Yin, H.; Cui, X.; Zhao, Y.; Zhang, J.; Tang, J.; Wang, F. A facile microwave hydrothermal synthesis of ZnFe₂O₄/rGO nanocomposites for supercapacitor electrodes. *Nanomaterials* **2023**, *13*, 1034. [[CrossRef](#)] [[PubMed](#)]
104. Yang, S.; Yue, W.; Zhu, J.; Ren, Y.; Yang, X. Graphene-based mesoporous SnO₂ with enhanced electrochemical performance for lithium-ion batteries. *Adv. Funct. Mater.* **2013**, *23*, 3570–3576. [[CrossRef](#)]
105. Lan, K.; Xia, Y.; Wang, R.; Zhao, Z.; Zhang, W.; Zhang, X.; Elzatahry, A.; Zhao, D. Confined interfacial monomeric assembly for precisely controlled coating of single-layered titania mesopores. *Matter* **2019**, *1*, 527–538. [[CrossRef](#)]
106. Tong, Z.; Liu, S.; Zhou, Y.; Zhao, J.; Wu, Y.; Wang, Y.; Li, Y. Rapid redox kinetics in uniform sandwich-structured mesoporous Nb₂O₅/graphene/mesoporous Nb₂O₅ nanosheets for high-performance sodium-ion supercapacitors. *Energy Storage Mater.* **2018**, *13*, 223–232. [[CrossRef](#)]

Disclaimer/Publisher's Note: The statements, opinions and data contained in all publications are solely those of the individual author(s) and contributor(s) and not of MDPI and/or the editor(s). MDPI and/or the editor(s) disclaim responsibility for any injury to people or property resulting from any ideas, methods, instructions or products referred to in the content.